J Appl Electrochem (2015) 45:1057–1068
DOI 10.1007/s10800-015-0879-z

RESEARCH ARTICLE

Platinum–rhodium–tin/carbon electrocatalysts for ethanol oxidation in acid media: effect of the precursor addition order and the amount of tin

F. E. López-Suárez[1] · M. Perez-Cadenas[2] · A. Bueno-López[3] · C. T. Carvalho-Filho[1] · K. I. B. Eguiluz[1] · G. R. Salazar-Banda[1]

Received: 25 April 2015 / Accepted: 27 July 2015 / Published online: 5 August 2015

Abstract Carbon-supported Pt_x–Rh_y–Sn_z catalysts (x:y:z = 3:1:4, 6:2:4, 9:3:4) are prepared by Pt, Rh, and Sn precursors reduction in different addition order. The materials are characterized by X-ray diffraction, transmission electron microscopy, and X-ray photoelectron spectroscopy techniques and are evaluated for the electrooxidation of ethanol in acidic media by cyclic voltammetry, chronoamperometry, and anode potentiostatic polarization. The influence of both the order in which the precursors are added and the composition of metals in the catalysts on the electrocatalytic activity and physicochemical characteristics of Pt_x–Rh_y–Sn_z/C catalysts is evaluated. Oxidized Rh species prevail on the surface of catalysts synthesized by simultaneous co-precipitation, thus demonstrating the influence of synthesis method on the oxidation state of catalysts. Furthermore, high amounts of Sn in composites synthesized by co-precipitation result in very active catalysts at low potentials (bifunctional effect), while medium Sn load is needed for sequentially deposited catalysts when the electronic effect is most important (high potentials), since more exposed Pt and Rh sites are needed on the catalyst surface to alcohol oxidation. The Pt_3–Rh_1–Sn_4/C catalyst prepared by co-precipitation is the most active at potentials lower than 0.55 V (related to bifunctional effect), while the Pt_6–Rh_2–Sn_4/C catalyst, prepared by sequential precipitation (first Rh and, after drying, Pt + Sn), is the most active above 0.55 V.

Keywords Bifunctional effect · Nanoparticles · Electrocatalysts composition · Electrocatalysis · Fuel cell

✉ F. E. López-Suárez
franzedwin@gmail.com

M. Perez-Cadenas
mariaperez@ccia.uned.es

A. Bueno-López
agus@ua.es

C. T. Carvalho-Filho
trivellatoc@hotmail.com

K. I. B. Eguiluz
katlin.eguiluz@pq.cnpq.br

G. R. Salazar-Banda
gianrsb@gmail.com

[1] Electrochemistry and Nanotechnology Laboratory, Research and Technology Institute/Processes Engineering Post-graduation - PEP, Universidade Tiradentes, Av. Murilo Dantas, 300, Aracaju, SE, Brazil

[2] Department of Inorganic and Technical Chemistry, Faculty of Sciences, UNED, Senda del Rey 9, 28040 Madrid, Spain

[3] MCMA Group, Department of Inorganic Chemistry, Faculty of Sciences, University of Alicante, Ap. 99, 03080 Alicante, Spain

1 Introduction

The electrocatalytic oxidation of small organic molecules to produce electrical energy by low-temperature direct fuel cell has received increasing attention due to its advantages with regard to other technologies, such as, easy transportation and storage of the fuel, reduced weight, size and complexity, and high energy efficiency. Ethanol is an attractive fuel for this application if compared with methanol and hydrogen, because it is less toxic, is available from renewable resources, and is easily stored and transported. However, the commercialization of direct ethanol fuel cells is hindered by the slow and inefficient alcohol oxidation on the available electrocatalysts [1, 2]. Platinum is the best catalyst for the adsorption and dissociation of

small organic molecules, but the activity for total electrooxidation (12 e^- per molecule) of ethanol to CO_2 is poor because (i) C–C bond cleavage is difficult and (ii) the oxidation rate of adsorbed reaction intermediates (CH_3CHO and CH_3COOH) is slow on the sites of Pt electrode [3–5].

Platinum is the best catalyst for the adsorption and dissociation of small organic molecules, but the activity for total electrooxidation (12 e^- per molecule) of ethanol to CO_2 is poor because (i) C–C bond cleavage is difficult and (ii) the oxidation rate of adsorbed reaction intermediates (CH_3CHO and CH_3COOH) is slow.

Bimetallic catalysts can improve the behavior of Pt-only electrocatalysts [6, 7]. Pt–Sn catalysts are generally considered the best anodes for ethanol oxidation, working at lower potentials than pure platinum [8–10]. Pt is the most active metal for alcohol oxidation in acid medium, and Sn provides surface oxygen species for the oxidation of CO and carbonyl species adsorbed on Pt, which are produced during the dissociative adsorption of ethanol on Pt active sites at low potentials [11–14]. The addition of Sn to Pt catalysts, although enhances the catalyst activity towards ethanol oxidation, cannot accelerate the C–C bond cleavage rate.

De Souza et al. [3] found that bimetallic Pt–Rh electrodes decrease the acetaldehyde yield and increase the CO_2 selectivity compared to pure platinum electrodes [10]. However, the ethanol oxidation rate achieved with Pt–Rh catalysts [15] rate is lower than that of Pt–Sn [10]. Ternary Pt–Rh-Sn electrocatalysts combine high oxidation rate with high CO_2 selectivity, and experimental and theoretical results demonstrate that the good performance of these ternary electrocatalysts is related to the synergistic effect of Pt, Rh, and Sn [10, 15–20]. Pt provides the active sites for the first reaction step, that is, the adsorption and dehydrogenation of ethanol. Rh plays the main role in decreasing the formation of acetaldehyde [21], and SnO_2 strongly adsorbs H_2O under electrochemical conditions, which provides OH^- for oxidation of CO adsorbed over Rh or Pt, keeping Pt and Rh available for further ethanol oxidation [18, 22–24].

Recent efforts have been concentrated on ternary Pt–Rh–Sn electrocatalyst [10, 15–20]. The preparation method is critical in order to achieve the desired activity, selectivity, and life-time of these systems [15, 25]. The synthesis strategies play a determining role in the catalyst properties including morphology, textures and forms, activity and stability, among others. For instance, Koval et al. [18, 20] synthesized Pt–Rh–SnO_2 nanoclusters supported on high-area carbon, with an optimum Pt:Rh:Sn atomic ratio of 3:1:4, by cation-adsorption/reduction-galvanic-displacement method. These catalysts showed to be very effective in C–C ethanol bond splitting at room temperature in acid solution and facilitate its oxidation to CO_2 at low potentials through oxametallacyclic conformation.

$Pt_{52}Sn_{(36-x)}Rh_{12}$–$Sn_xO_{2x}$ catalysts synthesized using a polyol process, with the coexistence of homogeneously distributed Pt/Sn/Rh random alloy and non-alloyed SnO_2 throughout the catalyst, possessed a superior long-term activity and stability towards ethanol oxidation than the commercial Pt catalyst [15]. Song et al. [16] reported a two-step synthesis of $PtSnO_2$@Rh/C catalysts by a modified pulse microwave-assisted polyol method followed by heat treatment, achieving an enhanced performance. They found that the as-obtained $PtSnO_2$@Rh/C catalyst exhibited high activity not only towards ethanol electrooxidation, but also towards further oxidation of its intermediate products (i.e., acetaldehyde and acetic acid).

Colmati et al. [10] synthesized carbon-supported ternary Pt–Sn–Rh (1:1:0.3 and 1:1:1) alloy catalysts by reduction of the metal precursors with formic acid concluding that, for potentials higher than 0.45 V (vs. reversible hydrogen electrode—RHE), the ternary Pt–Sn–Rh alloy catalysts possess the highest activity for ethanol electrooxidation, while for potentials lower than 0.45 V (vs. RHE), the electrochemical activity of the ternary catalysts was lower than that of the binary Pt–Sn catalyst.

Therefore, the development of electrocatalysts for ethanol oxidation to CO_2 is a major challenge in electrocatalysis. In this study, the effect of Pt–Rh–Sn electrocatalysts composition was investigated together with the effect of the Pt, Rh, and Sn addition order on the ethanol oxidation reaction (EOR) activity. Six Pt_x–Rh_y–Sn_z/C catalysts were prepared using co-precipitation reduction method and formic acid as reducing agent. The Pt:Rh atomic ratio was constant, and Sn content was modified. Besides, the addition order during the synthesis was varied in order to find the ternary optimal composition and the effect of preparation methodology. The structure and morphology of the catalysts were studied by X-ray diffraction (XRD), X-ray photoelectron spectroscopy (XPS), and transmission electron microscopy (TEM). The electrochemical properties, as well as the catalytic activity, were evaluated using cyclic voltammetry (CV), chronoamperometry (CA), and quasi-stationary potentiostatic polarization.

2 Experimental

2.1 Preparation of catalysts

All Pt_x–Rh_y–Sn_z/C electrocatalysts were prepared with a 20 % noble metal loading on the XC-72 carbon black support (Cabot Cop., 240 $m^2\ g^{-1}$). Pt_x–Rh_y–Sn_z/C catalysts with different atomic ratios (x:y:z = 3:1:4, 6:2:4,

9:3:4) were prepared by reduction of Pt, Rh, and Sn precursors through (i) sequential reductive precipitation (two-step sequence), first adding Rh and then Pt and Sn [called Pt_x–Rh_y–Sn_z/C—(S)] and, (ii) Pt and Sn were co-precipitated in one step [called Pt_x–Rh_y–Sn_z/C—(T)]. The 3:1 ratio of Pt:Rh was fixed in this study based on results presented in previous reports [3, 18] where it was established that higher Pt content with regard to Rh facilitates the C–C bond breaking on this system. Further reasons for using less Rh than Pt are that Rh alone is inactive for ethanol oxidation, and that it is even more expensive than Pt.

Catalysts were synthesized by a precipitation method using formic acid as reducing agent [26, 27]. For catalysts prepared in a two-step sequence, Rh/C was firstly obtained by the following procedure. The carbon support was added to a 2 M formic acid solution and heated to 85 °C, and then an appropriate amount of $RhCl_3{\cdot}xH_2O$ was added and mixed with the solution, and the slurry was maintained at 85 °C for 6 h. The suspension was cooled down to room temperature, and the powder was recovered by filtration, washed with ultrapure water until no chloride ions could be detected, and dried at 60 °C. This process was repeated afterwards with Rh/C and using $H_2PtCl_6{\cdot}6H_2O$ and $SnCl_2{\cdot}3H_2O$ as Pt and Sn precursors (Sigma Aldrich, purity >98 %), respectively. While for catalysts prepared in a one step, Pt and Sn precursors were added together with Rh/C already prepared.

2.2 Catalysts characterization

The crystalline structure was determined by XRD in a Seifert powder diffractometer using CuKα radiation (0.15418 nm). The diffractograms were registered at 2θ angles from 10 to 90°, with a step of 0.02° and a time per step of 3 s. The working conditions of the powder diffractometer were 1600 kW, a tension of 40 kV, and a current of 40 mA.

XPS characterization was carried out in a VG-Microtech Multilab 3000 electron spectrometer using Mg–Kα (1253.6 eV) radiation. To obtain the XPS spectra, the pressure of the analysis chamber was maintained at 5×10^{-10} mbar, and the binding energy (BE) scale was adjusted by setting the C1s transition to 284.6 eV.

Transmission electron microscopy images were obtained using a JEOL (JEM-2010) microscope at 200 kV. A few droplets of an ultrasonically dispersed suspension of each catalyst in ethanol were deposited on a copper grid with lacey carbon film and dried at ambient conditions for TEM characterizations. Particle size distributions were determined by using ~200 particles for each catalyst.

2.3 Electrochemical measurements

Electrochemical measurements were performed at room temperature using an Autolab Model PGSTAT 302N potentiostat/galvanostat. Experiments were carried out in a glass cell (one compartment) using a conventional three-electrode configuration (half-cell). The electrocatalyst was ultrasonically mixed with isopropyl alcohol (1 ml) and 30 µl Nafion® solution (5 wt% Aldrich solution) to form a uniform ink. Then, 5 µl of catalyst suspension was dropped onto a polished glassy carbon (GC) disk to form a homogenous thin catalyst layer. The reference system consisted of a hydrogen electrode in the same solution (HESS) connected by a Luggin capillary, and a Pt coil (0.25 cm^2) was used as the counter-electrode. All potentials were referred to the reversible hydrogen electrode (RHE). Nitrogen gas was bubbled through all solutions for 15 min before starting each electrochemical test.

Electrochemical activity tests were performed at room temperature in aqueous 0.5 M H_2SO_4 solutions containing 0.5 M C_2H_5OH. Cyclic voltammetry experiments were performed between 0.0 and 0.8 V until stationary responses were obtained. Then, two voltammetric cycles were performed between 0.0 and 1.0 V at 0.02 V s^{-1} to evaluate the behavior of each electrocatalyst. Chronoamperometric experiments were performed at 0.5 V, and anode polarization curves were obtained between 0.2 and 0.8 V in the potentiostatic mode, with all data points obtained after 200 s of polarization at each potential. The current densities were obtained by dividing the obtained current (in Amperes) by the geometric area of glassy carbon disk (in square centimeter) and per the amount of platinum present on catalyst (in grams). The tests were repeated for three times to check reproducibility.

The CO voltammetric stripping experiments were performed as follows. CO was adsorbed onto the electrode surface by bubbling high-purity CO through 0.5 M H_2SO_4 solution, while holding the electrode potential at 0.05 V. After the adsorption period (5 min), the dissolved CO was removed from the solution by bubbling high-purity nitrogen through the solution for 30 min keeping the potential at 0.05 V. The potential was then scanned in a positive direction from 0.05 V to 1.0 V at 0.01 V s^{-1}.

3 Results and discussion

3.1 Physico-chemical characterization of the electrocatalysts

3.1.1 XRD characterization

Figure 1a and b shows the XRD patterns of the catalysts prepared in one and two steps, respectively. The diffraction

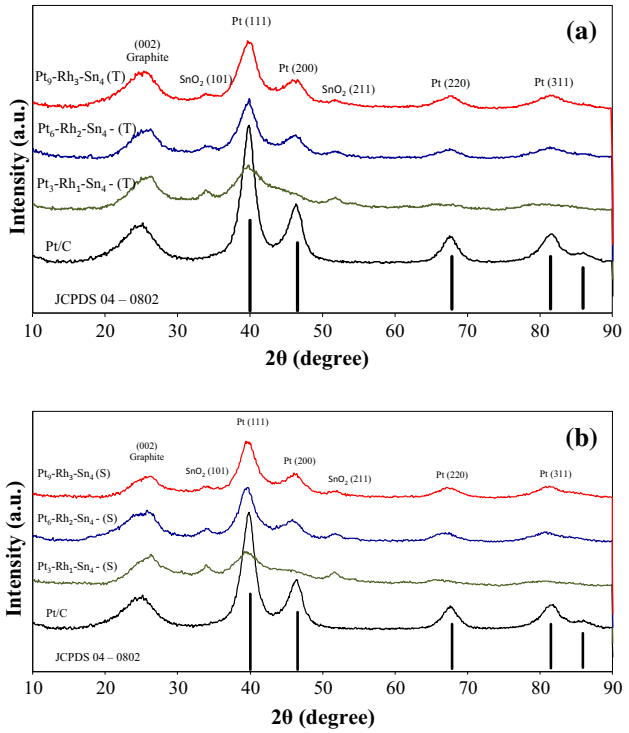

Fig. 1 X-ray diffractograms of samples over the scan range 10–90°. **a** Catalyst prepared by sequential precipitation, Pt_x–Rh_y–Sn_z/C—(**S**) and, **b** Pt and Sn co-precipitated, Pt_x–Rh_y–Sn_z/C—(**T**)

peak at 20–25° observed in all the diffraction patterns of the carbon-supported catalysts is attributed to the (002) plane of the hexagonal structure of Vulcan XC-72 carbon. The XRD patterns of all the catalysts show the characteristic peaks of the face-centered cubic (*fcc*) crystalline Pt with (111), (200), (220), and (311) planes appearing at the expected diffraction angles in good agreement with the Pt standard (JCPDS PDF 04-0802 reference included in Fig. 1). The diffraction peaks at 33° and 51° are assigned to SnO_2 (101) and (211) planes, respectively, indicating that Sn has been introduced into Pt_x–Rh_y–Sn_z/C catalysts as SnO_2. No peaks of metallic Rh or Rh oxides were detected in the Pt_x–Rh_y–Sn_z/C catalysts, but their presence cannot be discarded because they may be present in a very small particle size or even in an amorphous form. Moreover, Rh has very similar lattice parameters than Pt, and it is difficult to distinguish their peaks [19].

All diffraction peaks are broad, indicating a very small average crystallite size. The average Pt particles size was calculated from the Gaussian-fitted Pt (220) peak according to Scherrer's equation, and the obtained values together with the lattice parameter are given in Table 1. Crystallite sizes in the ~2.6–2.8 nm range were obtained for all Pt_x–Rh_y–Sn_z/C catalysts. The lattice parameters of the ternary catalysts were larger than that of Pt/C and all diffraction peaks shifted to lower 2θ values angles compared with Pt/C, further confirming the formation of a Pt-containing alloy and interactions between Pt and other metals, Sn and Rh. However, the opposite effects on lattice contraction/expansion induced by Rh and Sn doping, as well as the peak broadening due to small size of the catalyst, hinder the analysis of the formation of any binary or ternary alloy between Pt, Sn, and Rh. Finally, we can establish from XRD results that not major differences between the crystal structure and the preparation method were found among catalysts.

3.1.2 TEM characterization

All the catalysts were examined by TEM imaging. Figure 2a–f shows the TEM images and the particle size distribution of Pt_x–Rh_y–Sn_z/C prepared by two methodologies. The particle sizes, and the corresponding standard deviations are included in Table 1.

TEM results show differences in morphology between catalysts prepared by the different procedure. When the Pt and Sn precursors are added together [Pt_x–Rh_y–Sn_z/C—(**T**)], the density of particles increases, which seem to have coalesced to form small aggregates. However, for catalysts prepared by sequential impregnation [Pt_x–Rh_y–Sn_z/C—(**S**)], small bright nanoparticles with nano-spheres shape can be seen uniformly dispersed over the carbon support. No significant changes in the metal particle size due to the composition or preparation procedure were found, and its effect can be, therefore, ruled out in the interpretation of the electrocatalytic results.

3.1.3 XPS characterization

XPS analysis provided information about catalyst surface composition. The oxidation states of Pt, Rh, and Sn were studied by XPS following the Pt 4*f*, Rh 3*d,* and Sn 3*p* transitions, respectively. The Pt $4f_{7/2}$ and $4f_{5/2}$ spectra are shown in Fig. 3. The broad profiles could be deconvoluted into four different peaks with maxima at 71.5, 73.0, 74.8, and 76.1 eV, which corresponded to different Pt oxidation states. The deconvoluted peaks centered at 73.0 and 76.1 eV could be attributed to the Pt^{2+} [28], while those at 71.6 and 74.8 eV were attributed to metallic Pt. The surface metallic state of platinum (Pt^0) would provide more suitable sites for ethanol electrooxidation than Pt^{2+} species [29], and the presence of Pt^0 is essential for high ethanol electrooxidation rate.

Figure 4 shows the Sn 3*d* spectra profiles. Pt_x–Rh_y–Sn_z/C catalysts have two peaks with binding energy at 487 and 495 eV assigned to Sn^{4+} species for $3d_{5/2}$ and $3d_{3/2}$ transitions, respectively [30]. There are also other two small peaks at 485.5 and 493.8 eV, which correspond to metallic Sn [31]. These signals could come from the core of the Sn particles. The presence of SnO_2 [and/or $Sn(OH)_4$] in the catalyst agrees with results obtained by XRD.

Table 1 Structural characteristic obtained from XRD and TEM

Catalyst	Particle size (nm)[a]	Lattice parameter (nm)	Average particle size from TEM (nm)
Pt/C	3.8	0.3914	3.89 ± 1.04
Pt_3–Rh_1–Sn_4—(T)	2.6	0.3955	2.75 ± 0.69
Pt_6–Rh_2–Sn_4—(T)	2.8	0.3918	3.04 ± 0.82
Pt_9–Rh_3–Sn_4—(T)	2.8	0.3925	3.26 ± 0.80
Pt_3–Rh_1–Sn_4—(S)	2.8	0.3983	2.98 ± 0.86
Pt_6–Rh_2–Sn_4—(S)	2.8	0.3945	3.45 ± 0.78
Pt_9–Rh_3–Sn_4—(S)	2.8	0.3924	3.70 ± 0.66

[a] Calculated from Pt (220) peak with the Scherrer's formula

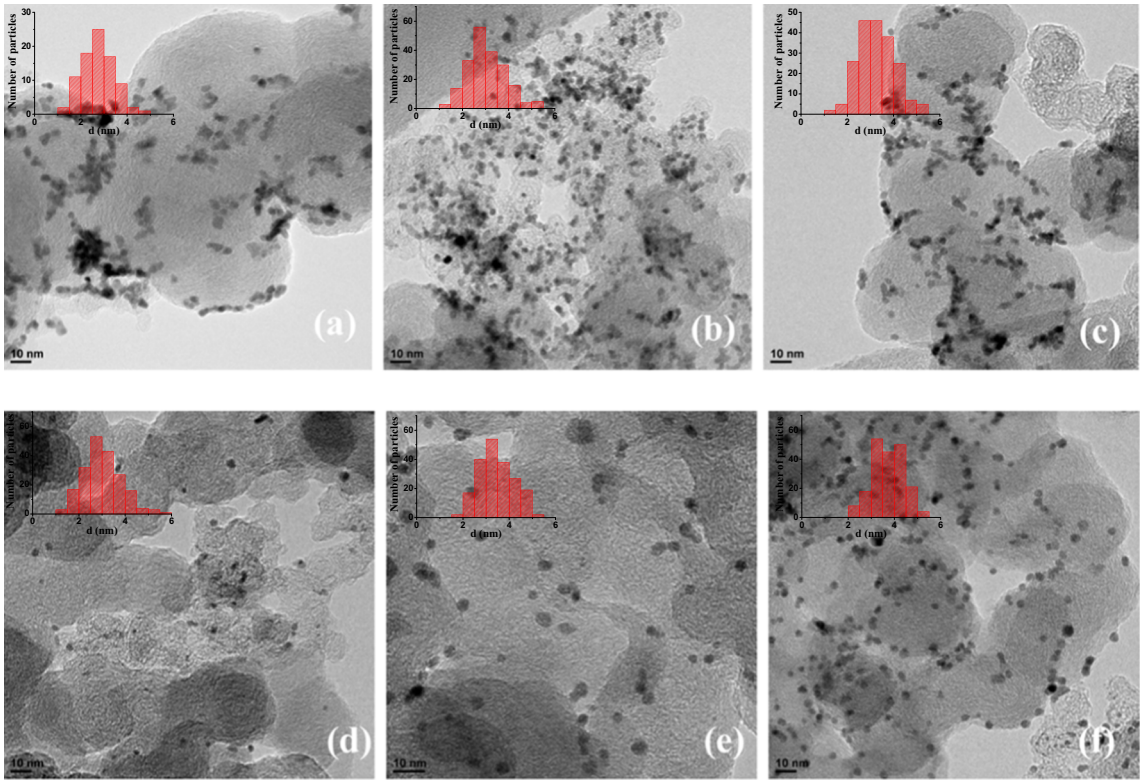

Fig. 2 TEM images and histogram of particle size distribution determined from TEM of Pt/C **a** Pt_3–Rh_1–Sn_4/C—(**T**), **b** Pt_6–Rh_2–Sn_4/C—(**T**), **c** Pt_9–Rh_3–Sn_4/C—(**T**), **d** Pt_3–Rh_1–Sn_4/C—(**S**), **e** Pt_6–Rh_2–Sn_4/C—(**S**), and **f** Pt_9–Rh_3–Sn_4/C—(**S**) catalysts

The Rh $3d_{5/2}$ and $3d_{3/2}$ spectra profiles are displayed in Fig. 5. Metal rhodium usually appears at ~307 and 312 eV, while oxidized rhodium species at ~309 and 313.5 eV [32]. In spite of the low surface rhodium concentration in some samples, which leads to noisy spectra, it is concluded that the position of the maxima for (T) samples is around 309 eV, which corresponds to cationic rhodium species, while the position for (S) samples is around 307 eV, being attributed to metallic rhodium. Thus, for Pt_x–Rh_y–Sn_z/C—(**T**) catalysts, oxidized Rh species are predominant on the surface, while for Pt_x–Rh_y–Sn_z/C—(**S**) catalysts, a major proportion of reduced Rh species are present.

Table 2 shows the percentage of the different Pt, Rh, and Sn species calculated from the relative intensities of deconvoluted peaks observed in the XPS spectra. The areas under the different deconvoluted Pt, Rh, and Sn peaks were quantified and normalized for all catalysts and the corresponding percentages calculated as a function of the total area. The results showed a prevailing presence of metallic Pt on the catalyst surfaces (~80 %) for all samples studied. The fraction of oxidized Pt species (~20 %) could be formed during catalyst exposure to the atmosphere, independently of the addition order of metal precursors. However, the percentage of reduced and oxidized Sn and Rh species depends on the preparation method. Oxidized

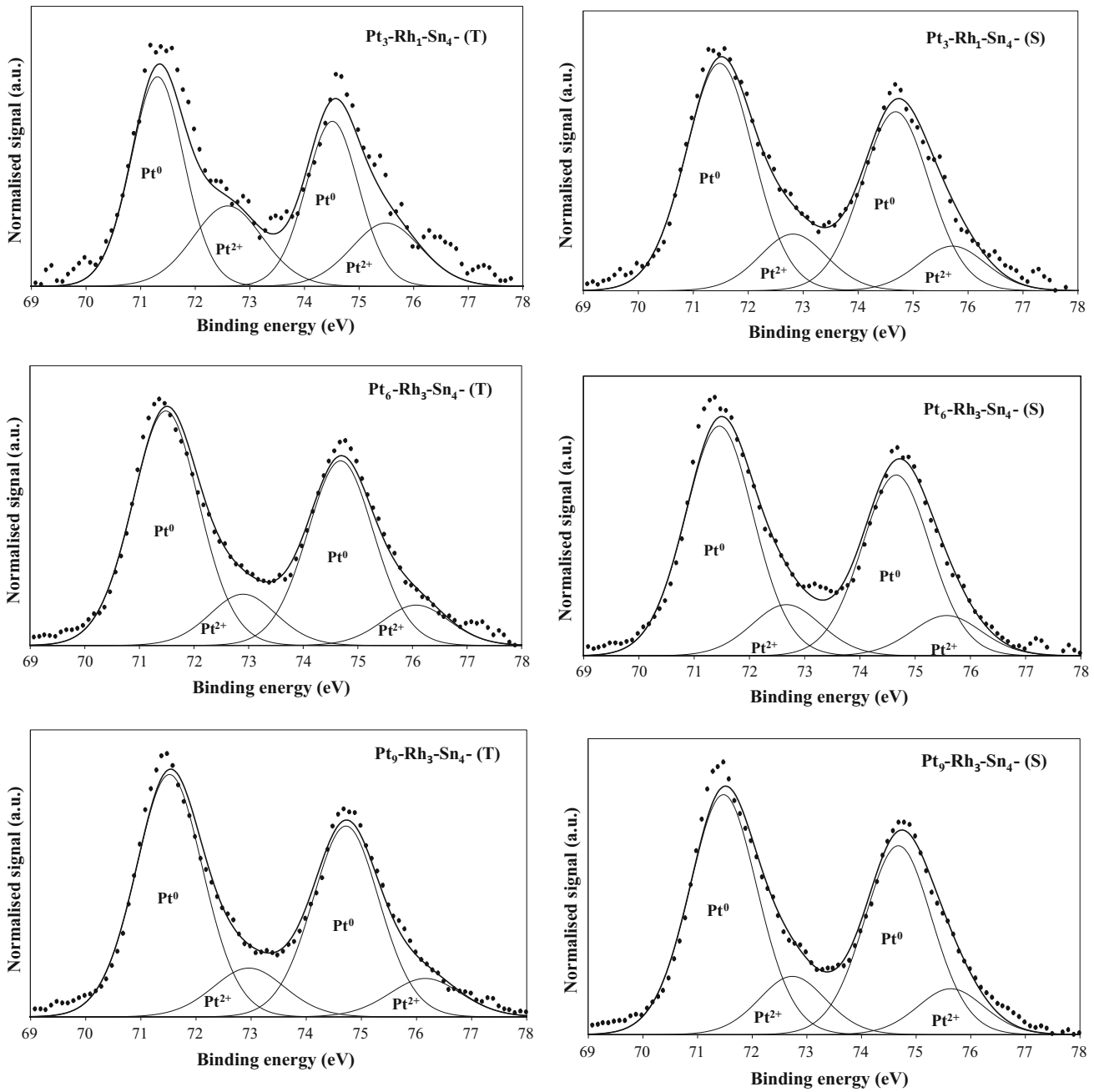

Fig. 3 Pt 4f transition in XPS experiments performed with catalysts

surface species prevail in catalysts prepared by simultaneous co-precipitation; meanwhile, the amount of reduced species on the surface is higher for catalysts prepared by sequential precipitation (see Table 2).

3.1.4 CO stripping

Figure 6 shows CO stripping voltammograms of catalysts recorded at 10 mV s^{-1} in the supporting electrolyte at room temperature. Currents are expressed in terms of geometric surface area. The tests were carried out with the most active electrocatalysts for ethanol electrooxidation (see next section), that is, Pt_3–Rh_1–Sn_4/C—(**T**) and (**S**) and Pt_6–Rh_2–Sn_4/C—(**S**), and with the reference Pt/C electrocatalyst. There is a single peak CO stripping anodic wave for the Pt/C catalyst, with an onset CO oxidation potential at 0.70 V and a maximum of the oxidation peak at 0.82 V. For Pt_x–Rh_y–Sn_z/C catalysts, there are two anodic waves for CO stripping, with the onset CO oxidation close to 0.30 V, and a broad stripping current peak at 0.55 V. The

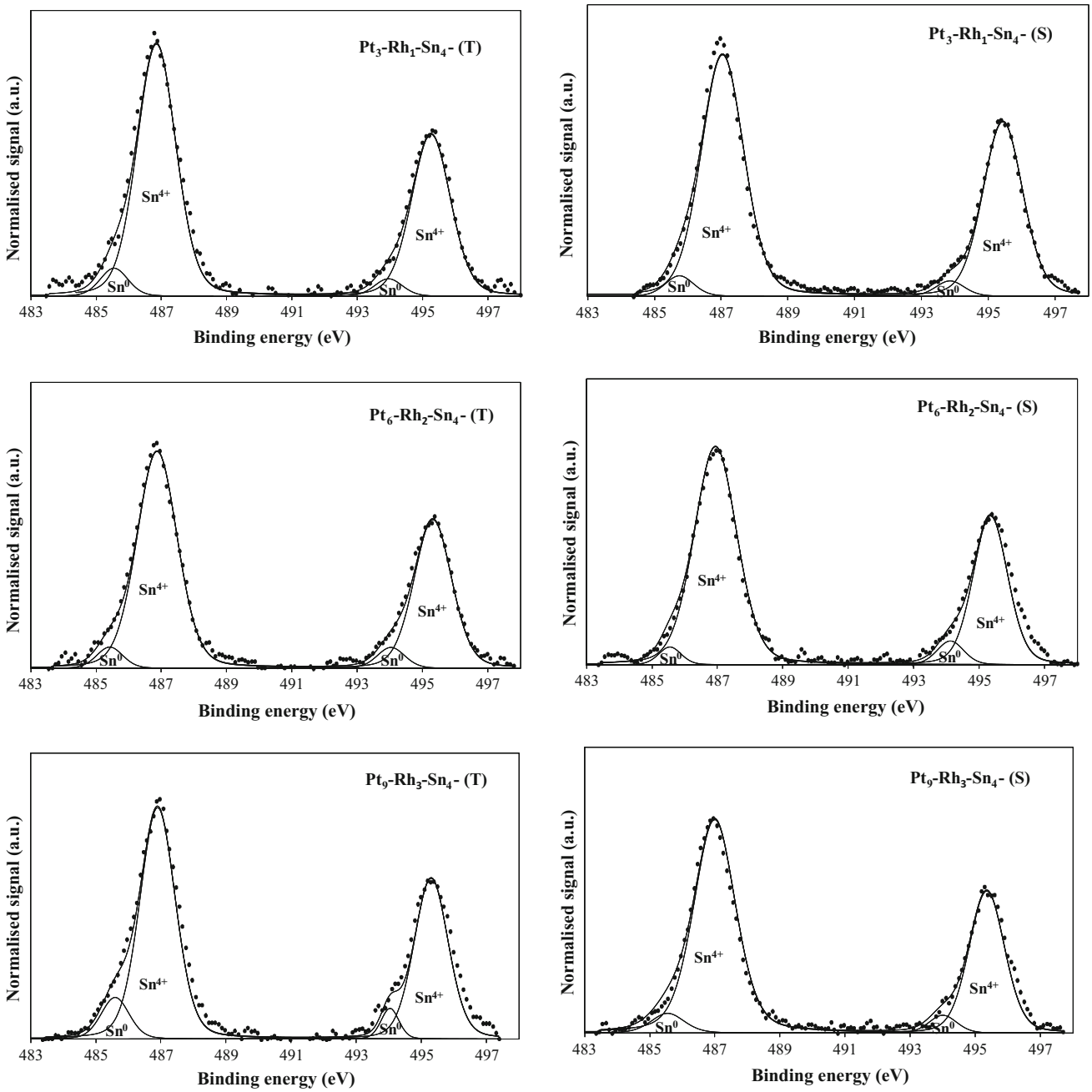

Fig. 4 Sn 3d transition in XPS experiments performed with catalysts

lower potential on the Pt_x–Rh_y–Sn_z/C catalysts is attributed to the presence of oxygenated species on Sn sites that are formed at lower potentials compared to platinum [33, 34], which allows the oxidation of CO to CO_2 at lower potentials according to the bifunctional mechanism [35]. The higher intensity showed for Pt_3–Rh_1–Sn_4/C—(**T**) and (**S**) catalysts at lower potentials is directly related to the higher amount of Sn on the catalyst. Different peaks and/or shoulders presented by CO stripping voltammograms could also be related to heterogeneous sites on the catalyst surface. The electrochemical active surface (EAS) areas were estimated assuming that the normalized charge density for a monolayer of adsorbed carbon monoxide on polycrystalline platinum is 420 μC cm^{-2} and that all platinum loaded on the working electrode is electrochemically active. The EAS values for Pt_3–Rh_1–Sn_4/C—(**T**) and (**S**), Pt_6–Rh_2–Sn_4/C—(**S**) and Pt/C catalysts were 33, 36, 37, and 21 cm^2 g^{-1}, respectively. An increase of EAS with the addition of Sn and Rh in the composition of the catalyst can be observed, so a higher amount of Pt is indeed

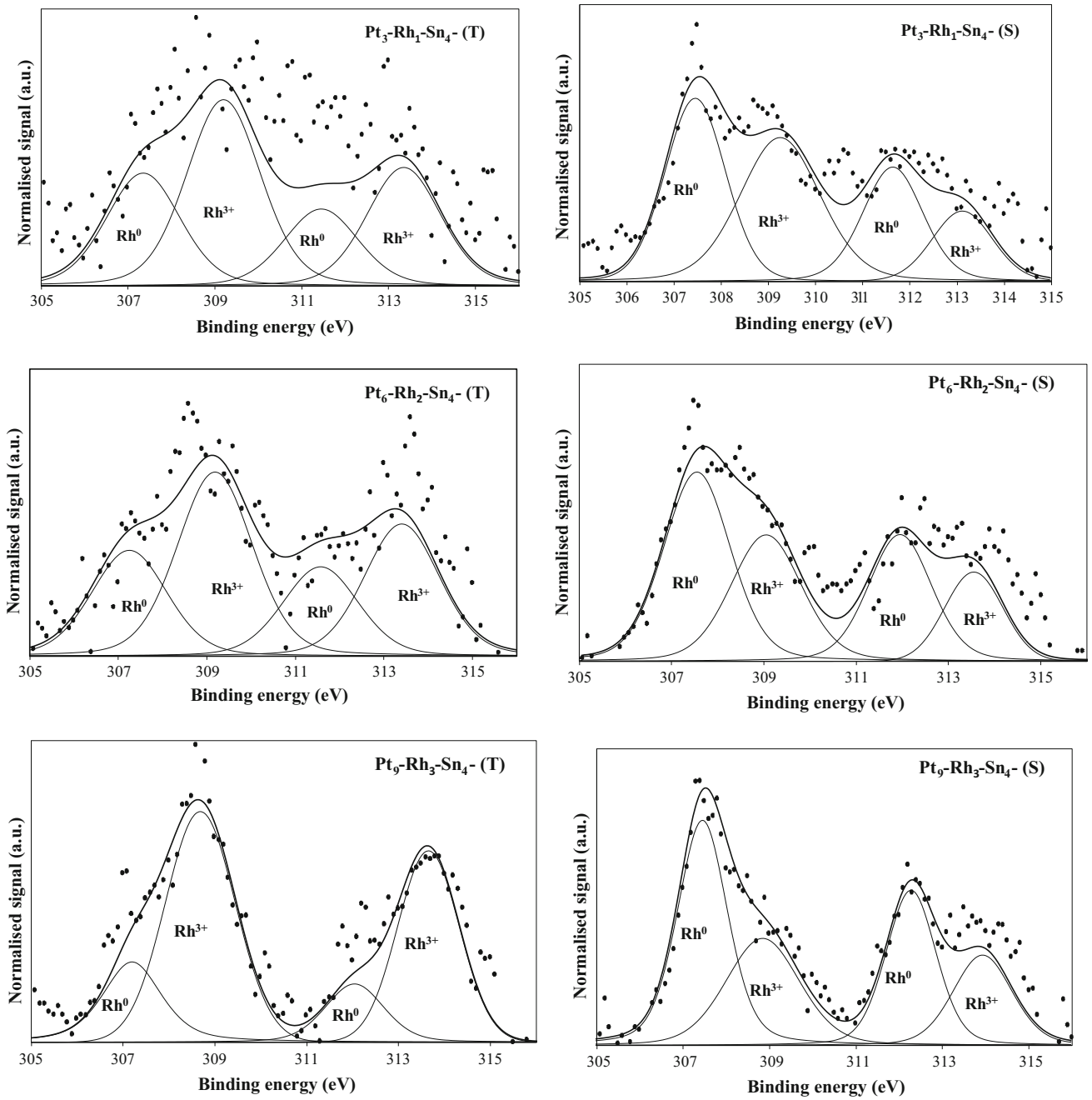

Fig. 5 Rh 3d transition in XPS experiments performed with catalysts

Table 2 Percentage of different Pt, Rh, and Sn species observed from the XPS data

Catalyst	Pt^0/Pt^{2+} species (%)	Sn^0/Sn^{2+} species (%)	Rh^0/Rh^{3+} species (%)
Pt/C	85/15	–	–
Pt_3–Rh_1–Sn_4—(T)	70/30	7/93	–
Pt_6–Rh_2–Sn_4—(T)	82/18	7/93	38/62
Pt_9–Rh_3–Sn_4—(T)	82/18	12/88	25/75
Pt_3–Rh_1–Sn_4—(S)	80/20	5/95	53/47
Pt_6–Rh_2–Sn_4—(S)	82/18	6/94	60/40
Pt_9–Rh_3–Sn_4—(S)	80/20	8/92	60/40

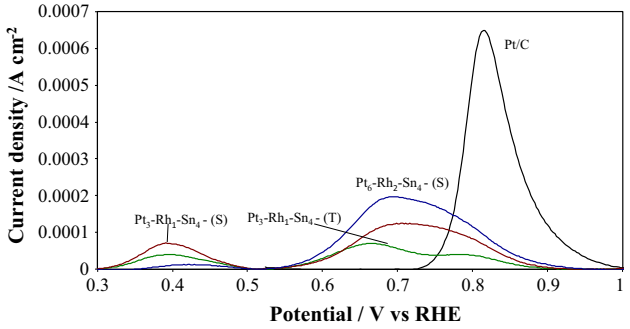

Fig. 6 CO stripping experiments recorded at 0.01 V s^{-1}

available where the EAS value was increased with respect to Pt/C.

3.2 Electrochemical experiments

Figure 7 shows cyclic voltammograms obtained in 0.5 M H_2SO_4 at a scan rate of 0.02 V s^{-1} (all catalysts), which show the typical behavior of hydrogen adsorption/desorption and oxide regions of Pt in acidic solutions [36]. The adsorption/desorption of hydrogen between 0.05 and 0.40 V was seen for all catalysts, but this region was not well defined for catalysts with high amount of Sn, i.e., Pt_3–Rh_1–Sn_4/C—(**T**) and (**S**). The hydrogen-desorption region for Pt_9–Rh_3–Sn_4/C—(**S**) was modified in comparison to Pt_9–Rh_3–Sn_4/C—(**T**), which depends predominantly on the preparation method. Finally, the structure of peaks in the electrochemical profiles for Pt_6–Rh_2–Sn_4/C—(**T**) and (**S**) catalysts was similar, independently of the preparation method. The presence of tin oxides on the particle surface increases electrode capacitance producing a large value for the double-layer charging current (0.4–0.7 V), indicating that all the catalysts have a similar double-layer charging current [37].

The electrocatalytic activities of the different catalysts during the oxidation of ethanol were compared by quasi-steady-state polarization and chronoamperometric measurements at room temperature. The anodic polarization curves of the catalysts in an ethanol-containing electrolyte showed in Fig. 8 indicate that the onset potential of ethanol electrooxidation using Pt_x–Rh_y–Sn_z/C was shifted negatively by ~0.2 V in comparison to Pt/C. For potentials lower than 0.55 V, the ternary Pt_3–Rh_1–Sn_4/C—(**T**) possesses the highest activity for ethanol electrooxidation, while for potentials higher than 0.55 V, the highest electrochemical activity of the ternary catalysts was for Pt_6–Rh_2–Sn_4/C—(**S**).

Notably, the electroactivity showed by catalysts with same composition, but with different preparation methodology, was lower for Pt_3–Rh_1–Sn_4/C—(**S**) and Pt_6–Rh_2–Sn_4/C—(**T**), than for Pt_3–Rh_1–Sn_4/C—(**T**) and Pt_6–Rh_2–Sn_4/C—(**S**), respectively. On the contrary, both the Pt_9–Rh_3–Sn_4/C—(**T**) and (**S**) catalysts presented very similar anodic polarization curves on the potential range studied. This behavior points out an important dependence between the metal precursors addition order and the composition of

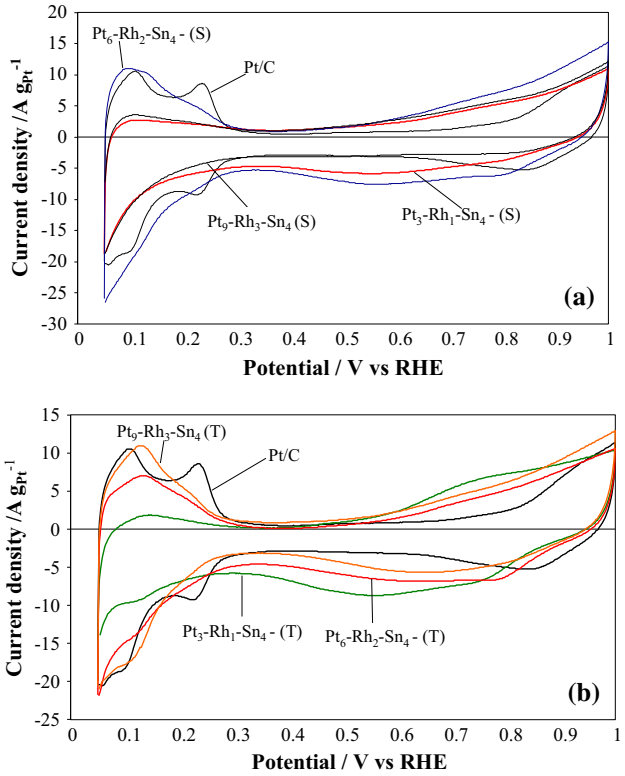

Fig. 7 Cyclic voltammetry curves for electrocatalysts in 0.5 M H_2SO_4 electrolyte. Scan rate of 0.02 V s^{-1} at room temperature. **a** Catalyst prepared by sequential precipitation, Pt_x–Rh_y–Sn_z/C—(**S**) and, **b** Pt and Sn co-precipitated, Pt_x–Rh_y–Sn_z/C—(**T**)

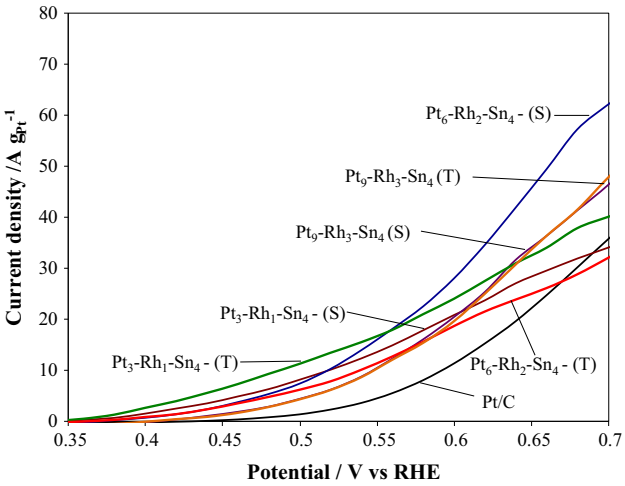

Fig. 8 Anode polarization profiles for the oxidation of ethanol in 0.50 M C_2H_5OH/0.5 M H_2SO_4 solutions at room temperature taken on the ternary electrocatalysts developed

the ternary Pt_x–Rh_y–Sn_z/C catalysts. A synergic effect between Pt, Sn, and Rh can be seen comparing the results obtained and displayed in Fig. 9 for binary catalysts (Pt_2–Sn_1/C and Pt_3–Rh_1/C) and Rh-containing catalysts. Figure 9 shows that the presence of Rh on the Pt_2–Sn_1/C catalyst leads to a substantial enhancement in the catalytic activity towards ethanol electrooxidation, in agreement with results reported by different authors [18, 19].

In the electrooxidation of ethanol at low temperature in acid environment [38] with platinum catalysts, the ability for C–C bond cleavage and CO oxidation are established as the rate-determining steps. Therefore, a synergic effect among all these three metals would be largely effective towards electrooxidation, as shown in Fig. 10, for chronoamperometry measurements performed at 0.5 V for Pt_x–Rh_y–Sn_z/C catalysts. During the first seconds, there was a sharp decrease in the current density, followed by a slow decrease in the current density, and a steady-state current was observed for all catalysts after ~400 s. This can be explained by the fact that, at first, dehydrogenation of ethanol occurs irreversibly on Pt sites leading to strongly adsorbed intermediates. Then, it seems that Sn favors CO–O coupling and also the oxidation of other adsorbed intermediates by providing oxygen, producing higher electrochemical currents. Rh modifies the Pt electronic properties and facilitates cleavage of C–C bonds.

The chronoamperometric curve for Pt/C displays a faster decrease than those for the other catalysts. The Pt_6–Rh_2–Sn_4/C—(**S**) catalyst presented higher activity, whereas similar behaviors for the Pt_3–Rh_1–Sn_4/C—(**T**) and Pt_3–Rh_1–Sn_4/C—(**S**) catalysts were seen. The lowest activity was presented by Pt_6–Rh_2–Sn_4/C—(**T**), Pt_9–Rh_3–Sn_4/C—(**T**) and (**S**) catalysts. A clear difference is displayed between Pt_6–Rh_2–Sn_4/C—(**S**) and (**T**) catalysts. After 600 s, the Pt_6–Rh_2–Sn_4/C—(**S**) catalyst displayed a value of pseudo-current density four times greater than that of Pt_6–Rh_2–Sn_4/C—(**T**) ($j = \sim 17$ A g_{Pt}^{-1} vs. $j = \sim 5$ A g_{Pt}^{-1}). Therefore, in accordance with the anodic polarization curves, there is a strong dependence between the metal precursors addition orders on the ternary Pt_x–Rh_y–Sn_z/C catalysts and the catalytic activity towards ethanol oxidation.

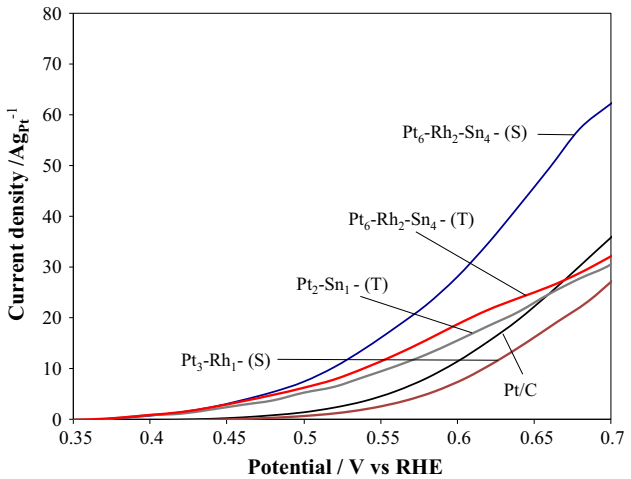

Fig. 9 Comparison of anode polarization profiles for the oxidation of ethanol in 0.50 M C_2H_5OH/0.5 M H_2SO_4 solution at room temperature for samples with Rh or without Rh

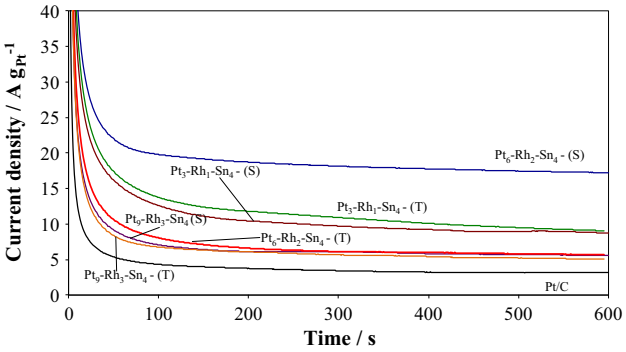

Fig. 10 Chronoamperometric curves for the oxidation of ethanol in 0.5 M C_2H_5OH/0.5 M H_2SO_4 solution at 0.5 V versus RHE at room temperature taken on the ternary electrocatalysts developed

The XRD, TEM, and XPS results showed that nanometer-sized noble metal catalysts can be easily prepared by two methods adopted here and both are suitable to prepare supported Pt–Rh–Sn-based catalysts with high metal loading. On the another hand, both the composition and the metal precursors addition order of the ternary Pt_x–Rh_y–Sn_z/C catalysts could modify the cooperative effect of Rh and Sn in the vicinity of Pt sites, and therefore could provide, or not, a high activity for ethanol oxidation and better tolerance towards poisoning species. The high activity of the Pt_6–Rh_2–Sn_4/C—(**S**) and Pt_3–Rh_1–Sn_4/C—(**T**) catalysts is attributed not only to the bifunctional effect of Pt and Sn (Pt provides active sites and Sn provides oxygenated species to oxidize the intermediates), but also to the electronic structure modified by ternary composition that facilitates C–C bonds cleavage, increasing the current density. It is worth to note that Rh is more expensive than Pt, and its use at low concentration can be justified because it increases the activity towards the electrooxidation of ethanol. While all the electrocatalysts investigated exhibited catalytic activity for ethanol oxidation, the most active one had the composition Pt:Rh:Sn = 6:2:4 atomic ratio prepared with the addition of metals separately (first Rh, and Pt–Sn afterwards).

4 Conclusions

A simple route was used to synthesize ternary Pt_x–Rh_y–Sn_z/C anode catalysts with different atomic ratio, by reduction of Pt, Rh, and Sn precursors in different addition order

using formic acid as reducing agent. The highest content of Sn used in the catalysts (Pt_3–Rh_1–Sn_4/C) results in high catalytic activity towards ethanol oxidation at low potentials (<0.55 V), independently of the synthesis methodology, which is attributed to the fact that Sn provides oxygenated species to oxidize the intermediates (bifunctional effect). Alternatively, the activity of Pt_6–Rh_2–Sn_4/C catalysts strongly depends on the synthesis conditions. The sequential reductive precipitation (two-steps) resulted in both, a major proportion of reduced Rh species and the highest catalytic activity at high potentials (>0.55 V). Possibly, the enhanced activity results from both, the bifunctional effect and the Pt electronic structure modified by Rh that facilitates C–C bonds cleavage. Thus, the crystal structure and the distribution Sn and Rh species on the catalyst surface depend on the preparation method. A correlation between the metal addition order and the composition of the ternary Pt_x–Rh_y–Sn_z/C catalysts towards ethanol electrooxidation was found. The catalytic properties of this ternary electrocatalyst might play an important role in ethanol oxidation, and this was attributed to the synergistic effect between all three constituents.

Acknowledgments The authors thank the Brazilian National Council of Technological and Scientific Development-CNPq (Grants: 402243/2012-9, 303630/2012-4, 474261/2013-1, 407274/2013-8, and 310282/2013-6) for the scholarships and financial support for this work.

References

1. Lamy C, Rousseau S, Belgsir E, Coutanceau C, Léger J-M (2004) Recent progress in the direct ethanol fuel cell: development of new platinum–tin electrocatalysts. Electrochim Acta 49(22):3901–3908
2. Antolini E (2007) Catalysts for direct ethanol fuel cells. J Power Sources 170(1):1–12
3. De Souza J, Queiroz S, Bergamaski K, Gonzalez E, Nart F (2002) Electro-oxidation of ethanol on Pt, Rh, and PtRh electrodes. A study using DEMS and in situ FTIR techniques. J Phys Chem B 106(38):9825–9830
4. Camara G, Iwasita T (2005) Parallel pathways of ethanol oxidation: the effect of ethanol concentration. J Electroanal Chem 578(2):315–321
5. Xia X, Liess H-D, Iwasita T (1997) Early stages in the oxidation of ethanol at low index single crystal platinum electrodes. J Electroanal Chem 437(1):233–240
6. Lamy C, Lima A, LeRhun V, Delime F, Coutanceau C, Léger J-M (2002) Recent advances in the development of direct alcohol fuel cells (DAFC). J Power Sources 105(2):283–296
7. Dubau L, Hahn F, Coutanceau C, Léger J-M, Lamy C (2003) On the structure effects of bimetallic PtRu electrocatalysts towards methanol oxidation. J Electroanal Chem 554:407–415
8. Prater KB (1996) Solid polymer fuel cells for transport and stationary applications. J Power Sources 61(1):105–109
9. Simões F, Dos Anjos D, Vigier F, Léger J-M, Hahn F, Coutanceau C, Gonzalez E, Tremiliosi-Filho G, De Andrade A, Olivi P (2007) Electroactivity of tin modified platinum electrodes for ethanol electrooxidation. J Power Sources 167(1):1–10
10. Colmati F, Antolini E, Gonzalez E (2008) Preparation, structural characterization and activity for ethanol oxidation of carbon supported ternary Pt–Sn–Rh catalysts. J Alloy Compd 456(1): 264–270
11. Vigier F, Coutanceau C, Perrard A, Belgsir E, Lamy C (2004) Development of anode catalysts for a direct ethanol fuel cell. J Appl Electrochem 34(4):439–446
12. Neto AO, Giz M, Perez J, Ticianelli E, Gonzalez E (2002) The electro-oxidation of ethanol on Pt–Ru and Pt–Mo particles supported on high-surface-area carbon. J Electrochem Soc 149(3): A272–A279
13. González Pereira M, Dávila Jiménez M, Elizalde MP, Manzo-Robledo A, Alonso-Vante N (2004) Study of the electrooxidation of ethanol on hydrophobic electrodes by DEMS and HPLC. Electrochim Acta 49(22):3917–3925
14. Camara G, De Lima R, Iwasita T (2004) Catalysis of ethanol electrooxidation by PtRu: the influence of catalyst composition. Electrochem Commun 6(8):812–815
15. Du W, Wang Q, LaScala CA, Zhang L, Su D, Frenkel AI, Mathur VK, Teng X (2011) Ternary PtSnRh–SnO_2 nanoclusters: synthesis and electroactivity for ethanol oxidation fuel cell reaction. J Mater Chem 21(24):8887–8892
16. Song S, He C, Liu J, Wang Y, Brouzgou A, Tsiakaras P (2012) Two-step sequence for synthesis of efficient PtSn@ Rh/C catalyst for oxidizing ethanol and intermediate products. Appl Catal B Environ 119:227–233
17. Li M, Cullen DA, Sasaki K, Marinkovic NS, More K, Adzic RR (2012) Ternary electrocatalysts for oxidizing ethanol to carbon dioxide: making Ir capable of splitting C–C bond. J Am Chem Soc 135(1):132–141
18. Kowal A, Li M, Shao M, Sasaki K, Vukmirovic M, Zhang J, Marinkovic N, Liu P, Frenkel A, Adzic R (2009) Ternary Pt/Rh/SnO_2 electrocatalysts for oxidizing ethanol to CO_2. Nat Mater 8(4):325–330
19. Li M, Kowal A, Sasaki K, Marinkovic N, Su D, Korach E, Liu P, Adzic R (2010) Ethanol oxidation on the ternary Pt–Rh–SnO/C electrocatalysts with varied Pt:Rh:Sn ratios. Electrochim Acta 55(14):4331–4338
20. Kowal A, Gojković SL, Lee K-S, Olszewski P, Sung Y-E (2009) Synthesis, characterization and electrocatalytic activity for ethanol oxidation of carbon supported Pt, Pt–Rh, Pt–SnO_2 and Pt–Rh–SnO_2 nanoclusters. Electrochem Commun 11(4):724–727
21. Jones GS, Mavrikakis M, Barteau MA, Vohs JM (1998) First synthesis, experimental and theoretical vibrational spectra of an oxametallacycle on a metal surface. J Am Chem Soc 120(13):3196–3204
22. Lima F, Gonzalez E (2008) Ethanol electro-oxidation on carbon-supported Pt–Ru, Pt–Rh and Pt–Ru–Rh nanoparticles. Electrochim Acta 53(6):2963–2971
23. Wang Y, Song S, Andreadis G, Liu H, Tsiakaras P (2011) Understanding the electrocatalytic activity of Pt_xSn_y in direct ethanol fuel cells. J Power Sources 196(11):4980–4986
24. Zhou W, Zhou Z, Song S, Li W, Sun G, Tsiakaras P, Xin Q (2003) Pt based anode catalysts for direct ethanol fuel cells. Appl Catal B Environ 46(2):273–285
25. Silva J, De Souza R, Parreira L, Neto ET, Calegaro M, Santos M (2010) Ethanol oxidation reactions using SnO_2@Pt/C as an electrocatalyst. Appl Catal B Environ 99(1):265–271
26. Colmati F, Antolini E, Gonalez ER (2007) Ethanol oxidation on carbon supported Pt–Sn electrocatalysts prepared by reduction with formic acid. J Electrochem Soc 154(1):B39–B47
27. Colmati F, Antolini E, Gonzalez ER (2007) Ethanol oxidation on a carbon-supported Pt75Sn25 electrocatalyst prepared by reduction with formic acid: effect of thermal treatment. Appl Catal B Environ 73(1):106–115

28. Sun S, Yang D, Villers D, Zhang G, Sacher E, Dodelet J-P (2008) Template-and surfactant-free room temperature synthesis of self-assembled 3D Pt nanoflowers from single-crystal nanowires. Adv Mater 20(3):571–574
29. Park K-W, Choi J-H, Lee S-A, Pak C, Chang H, Sung Y-E (2004) PtRuRhNi nanoparticle electrocatalyst for methanol electrooxidation in direct methanol fuel cell. J Catal 224(2):236–242
30. Shukla A, Arico A, El-Khatib K, Kim H, Antonucci P, Antonucci V (1999) An X-ray photoelectron spectroscopic study on the effect of Ru and Sn additions to platinised carbons. Appl Surf Sci 137(1):20–29
31. Zignani S, Gonzalez E, Baglio V, Siracusano S, Aricò A (2012) Investigation of a Pt3Sn/C electro-catalyst in a direct ethanol fuel cell operating at low temperatures for portable applications. Int J Electrochem Sci 7:3155–3166
32. Hakeem AA, Rajendran J, Kapteijn F, Makkee M (2015) Effect of rhodium on the water–gas shift performance of Fe_2O_3/ZrO_2 and CeO_2/ZrO_2: influence of rhodium precursor. Catal Today 242:168–177
33. Morimoto Y, Yeager EB (1998) CO oxidation on smooth and high area Pt, Pt–Ru and Pt–Sn electrodes. J Electroanal Chem 441(1):77–81
34. Wang K, Gasteiger H, Markovic N, Ross P (1996) On the reaction pathway for methanol and carbon monoxide electrooxidation on Pt–Sn alloy versus Pt–Ru alloy surfaces. Electrochim Acta 41(16):2587–2593
35. Gasteiger HA, Markovic N, Ross PN Jr, Cairns EJ (1994) Carbon monoxide electrooxidation on well-characterized platinum-ruthenium alloys. J Phys Chem 98(2):617–625
36. Stevens D, Dahn J (2003) Electrochemical characterization of the active surface in carbon-supported platinum electrocatalysts for PEM fuel cells. J Electrochem Soc 150(6):A770–A775
37. Chang SC, Leung LWH, Weaver MJ (1990) Metal crystallinity effects in electrocatalysis as probed by real-time FTIR spectroscopy: electrooxidation of formic acid, methanol, and ethanol on ordered low-index platinum surfaces. J Phy Chem 94(15):6013–6021
38. Kua J, Goddard WA (1999) Oxidation of methanol on 2nd and 3rd row group VIII transition metals (Pt, Ir, Os, Pd, Rh, and Ru): application to direct methanol fuel cells. J Am Chem Soc 121(47):10928–10941